Rotor Wake/Fixed Wing Interactions with Flap Deflection

Catherine Matos, Urmila Reddy, Narayanan Komerath
School of Aerospace Engineering
Georgia Institute of Technology
Atlanta, GA

ABSTRACT

The basic features in the interaction of a rotor wake with a wing in low-speed forward flight are studied using low-speed wind tunnel experiments. The configuration captures several of the aerodynamic interactions in the tiltrotor transition phase, and during wake/empennage interactions. Previous work showed that the pressure field on the wing surface below the rotor is dominated by n-per-rev "blade passage", while the velocity field is dominated by once-per-rev repetition of the vortex geometry, due to vortex interactions. The effect of deflecting trailing edge flaps is studied here. Large area SCV is used to enable velocity field acquisition at various sections and test conditions. Flap deflection modifies the spanwise flow on the wing surface, and causes an apparent lateral shift in the wake interaction. This shift influences the effectiveness of inboard vs. outboard flaps, and opens possibilities for augmenting rolling moments. The paper describes both a unique capability for scanning several cross-sections of a periodic velocity field during such interaction conditions, and the correlation of data from velocity, pressure and force measurements to synthesize the nature of the complex flowfield with its multiple periodicities.

INTRODUCTION

During hover and transition, wake-induced download on the wings of a tiltrotor aircraft is mitigated, and lift is enhanced, by deflecting wing trailing edge flaps. Wake / lifting surface interactions are also important in predicting empennage buffeting. The experiment described here is a basic test case of rotor wake/ lifting surface interaction, where various phenomena are visualized, isolated, quantified, and modified. Figure 1 shows the relation between the tiltrotor case, and the basic full-span wing-rotor configuration in the wind tunnel. The retreating blade side on the wing surface is analogous to the wing of the tiltrotor.

The rotor-wing set-up in the John Harper wind tunnel at Georgia Tech is shown in Figure 2. A full-span NACA0021 wing with 0.4 m chord at a 0 degree angle of attack is centered about the rotor axis. It is mounted on a stand below a 0.914 m diameter, two-bladed teetering rotor. The rotor is mounted on the tunnel roof with its hub at 0.127 m upstream of the wing leading edge and centered at mid-span. The rotor hub is at a height of 0.4191 m above the wing centerline. Two trailing edge flaps were used in this experiment. The first was a full-span cambered flap with a 0.125 m chord is attached to the trailing edge of the wing. The second was a flap system, consisting of 4 computer controlled NACA0012 flap segments with a 0.127 m chord. Computer control of the flaps allowed them to be independently deflected to various angles from outside the windtunnel. The rotor was run at 1050 RPM and an advance ratio of 0.075 was maintained by keeping the tunnel freestream steady at 3.77 m/s.

The conceptual difficulty of transposing results to the tiltrotor, due to the presence of the wing under the advancing blade side (ABS), is balanced by the efficiency of understanding what the rotor wake does when it interacts with an easily-modeled full-span lifting surface. Likewise, the wake vortex system behavior is better understood by considering a 2-bladed, untwisted rotor even though there are no 2-bladed tiltrotor craft under official consideration. Future load-modification tests, using the basic results from the present experiments, will use a half-span wing with suitable controls, in combination with a 2-bladed rotor and then a 3-bladed, twisted

---

Presented at the American Helicopter Society 55th Annual Forum, Montreal, Canada, May 25-27, 1999.

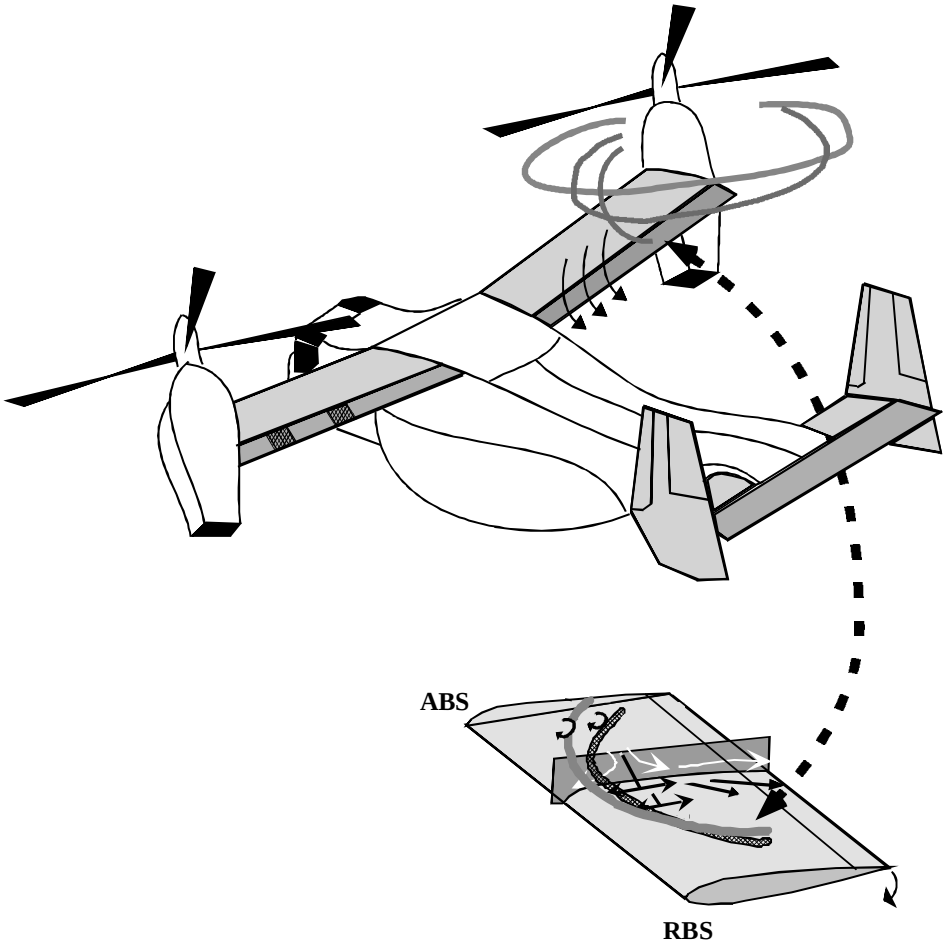

Figure 1: Relationship between tiltrotor case and full-span wing-rotor experiment

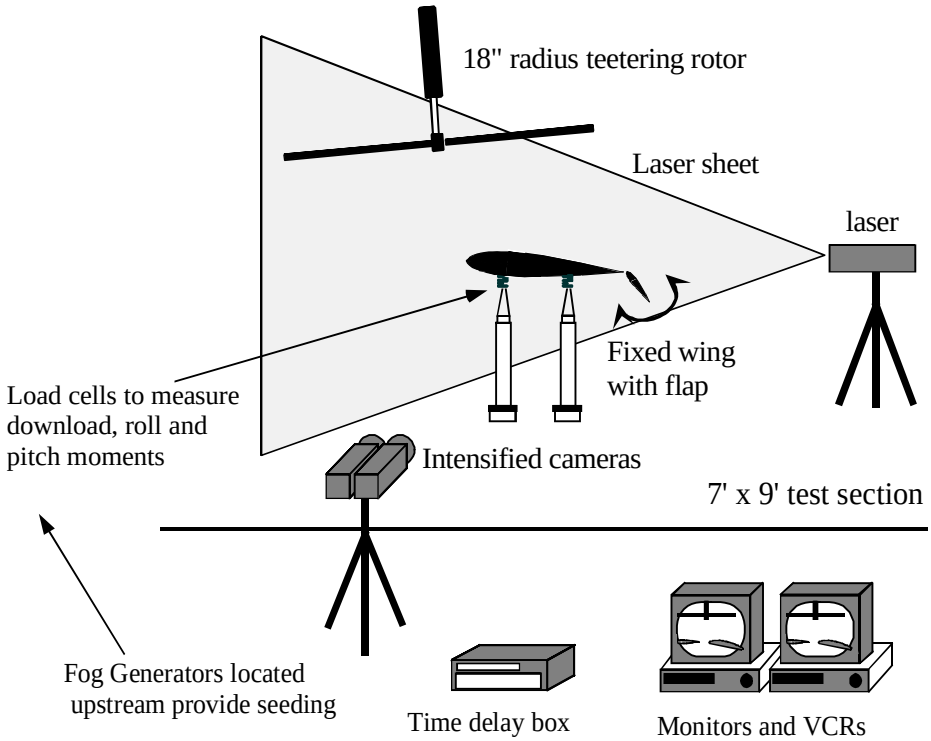

Figure 2: Experimental Setup

prop-rotor scale model. Tests conducted at industry sites on actual tiltrotor models provide a separate route to relate low-speed, basic results to those obtained from scale models and from tests at full-scale Reynolds and tip Mach number, where detailed diagnostics are more difficult.

The flowfield in the rotor wake/wing interaction region is dominated by interacting tip vortices and vortex sheets, with large-amplitude, periodic variations in each component. Two well-known features from previous work, using scale-model and full-scale tests [1], are:

a. The wake interaction with the wings produces a strong spanwise flow. In the case of the tiltrotor, the spanwise flows from the two rotors interact, and develop into a "fountain effect" which has been suspected as one cause of BVI noise.

b. Flap deflection alleviates the download on the wings.

These features are also predicted by state-of-the-art computer codes. However, it would be interesting to see if present-day codes predict the unsteady aspects of the problem, and some manifestations of these aspects:.

Earlier phases of the present experiment showed that [2]:

1. There is a strong n-per-rev loading on the wing due to the pressure distributions of the moving blades, and their interaction with the wing surface.
2. Wing interaction causes a large divergence in the trajectories of tip vortices from the different blades, so that the flowfield shows a strong once-per-rev component superposed on the n-per-rev.
3. When the tip vortices reach the wing surface, they induce transient flow separation on the upper surface, as well as high levels of spanwise velocity downstream of the separation line.

Detailed velocity measurements in the mid-span vertical plane above the wing, performed by Funk [7], had shown the periodicity of the velocity field. Except during the final stages of vortex interaction with the surface, the flow is quite cleanly periodic (whether at one per rev or n per rev), with very small root-mean-square values of fluctuation about the periodic value, in every 1-degree interval of rotor azimuth.

Each of the above three results is illustrated below. Figure 3 shows the divergence in the trajectories of the tip vortices from the two rotor blades. The image in the background is a video image of smoke behavior in a thin section illuminated by a light sheet from a copper vapor laser. The trajectory superposed on the image was obtained by digitizing a few images and plotting the position of the vortex center as a function of rotor azimuth. Earlier experiments by Funk et al [3] had shown that this divergence is due to interaction between the two vortices, aggravated by the presence of the wing. These effects are predictable using simple vortex dynamics and potential flow theory.

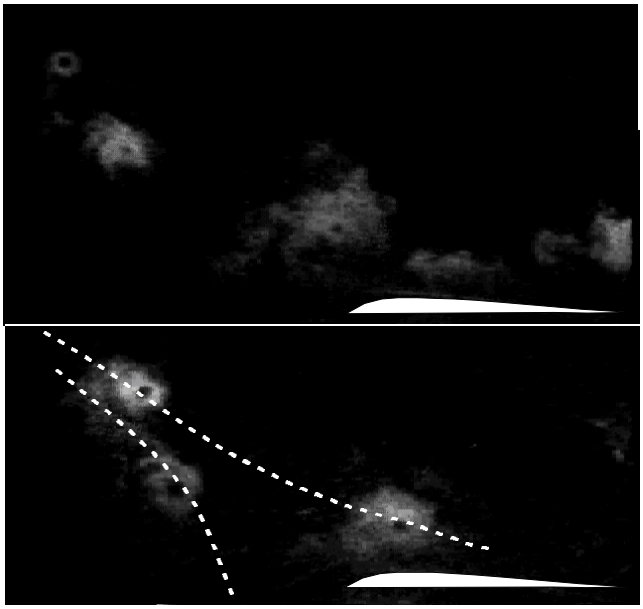

Figure 3: Vortex trajectories over the leading edge of the wing.

Figure 4 shows the quasi-steady values of section lift coefficient obtained by Funk [7] along chordwise lines at different stations along the span of the wing. These values were obtained by integrating the unsteady pressures measured using flush-mounted microphones located on the upper and lower surfaces. The lift coefficient shows a clear 2-per rev variation, with a small 1-per rev sub-harmonic. The average of a large number of revolutions (which smears out the non-periodic parts of the signal) is close to the value for the last cycle of the data.

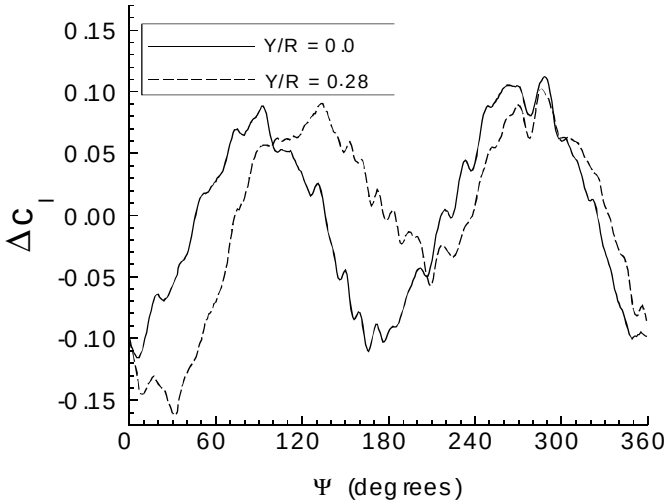

Figure 4: Variation in sectional lift coefficient

Figure 5a shows the two-dimensional velocity field and vorticity contours obtained from pointwise LDV measurements. Flow separation is evident at the location where the tip vortex impinges on the wing surface. Further downstream however the flow appears to remain attached. This is explained by the presence of the strong spanwise flow shown schematically in Figure 5b. This schematic summarizes results from tuft visualizations by Funk [7]. There are regions of outward flow on both the RBS and the ABS, with the dividing lines between inward and outward flows shown in the figure. Due to the spanwise flow over the aft portions of the wing, the velocity field is substantially attached over the wing, except for the 3-D separation line upstream of the vortex interactions.

In the present experiment, the effect of flap deflection on the forces, moments, pressure distribution and unsteady velocity field of the basic wing-rotor experiment is studied in a wind tunnel. The daunting measurement challenges of quantifying the velocity field for various settings of the flaps, as a function of rotor azimuth, at several spanwise locations, are approached using the planar Spatial Correlation Velocimetry (SCV) technique. SCV has been applied to quasi-steady and unsteady, 2-D flows with laser illumination [3,4] and 3-D unsteady rotorcraft flows with white light sheets at full-scale tip Mach number and measurement distance [5]. The different aspects of the technique have been validated using solid surface displacement and addition of random measurement noise [3], and point velocity measurements [6].

The flow field is scanned in a number of "slices" using SCV, and the resulting velocity fields are sorted into "bins" of rotor phase, and the periodic velocity field is obtained. Pressure taps are used to determine the mean pressure over the wing for each flap deflection case. The wing-flap system is mounted on four compression/tension load cells to record variations in average download and moments on the wing due to different flap deflections.

EXPERIMENTAL DETAILS

The split flap system was attached to the trailing edge of the wing, and deflected using push-pull rods. Each flap could be independently controlled, and cover a minimum deflection range of -15 to 45 degrees. Four S-type load cells were used to record download on the wing with an uncertainty of 0.04%, (< 0.02lbs). The load cells formed the top part of the stand that the wing was situated on. Load cells were located 0.178 m apart in the chordwise direction, and 1.232 m apart in the spanwise direction. The static pressure distribution over the surface was also measured, with the rotor running at 2100 RPM and maintaining the same advance ratio of 0.075.

Two intensified CCD cameras aligned to the same object field, recorded the seeded flowfield section, which was illuminated by argon ion or pulsed white-light sheets. A third camera tracked the rotor azimuth. A smoke rake 2.54 m upstream of the rotor hub seeded the flow with theatrical fog (condensing particles of propylene glycol derivative). The measurement plane was held at each station for roughly 30 seconds to record a range of rotor azimuths and then traversed across the flowfield to the next station.

RESULTS

1. Lateral Shift of the Rotor Wake Due to Flap Deflection:

Contours of the pressure coefficient on the wing surface on the RBS, referenced to freestream dynamic pressure, are plotted in Figure 6 for (a) 0 degree flap deflection, and (b) 27 degree flap deflection. The rotor wake impinging on the wing causes a large region of positive pressure, with pressure coefficients about 2.0. The contours with the flap deflected show a decrease of mean pressures throughout

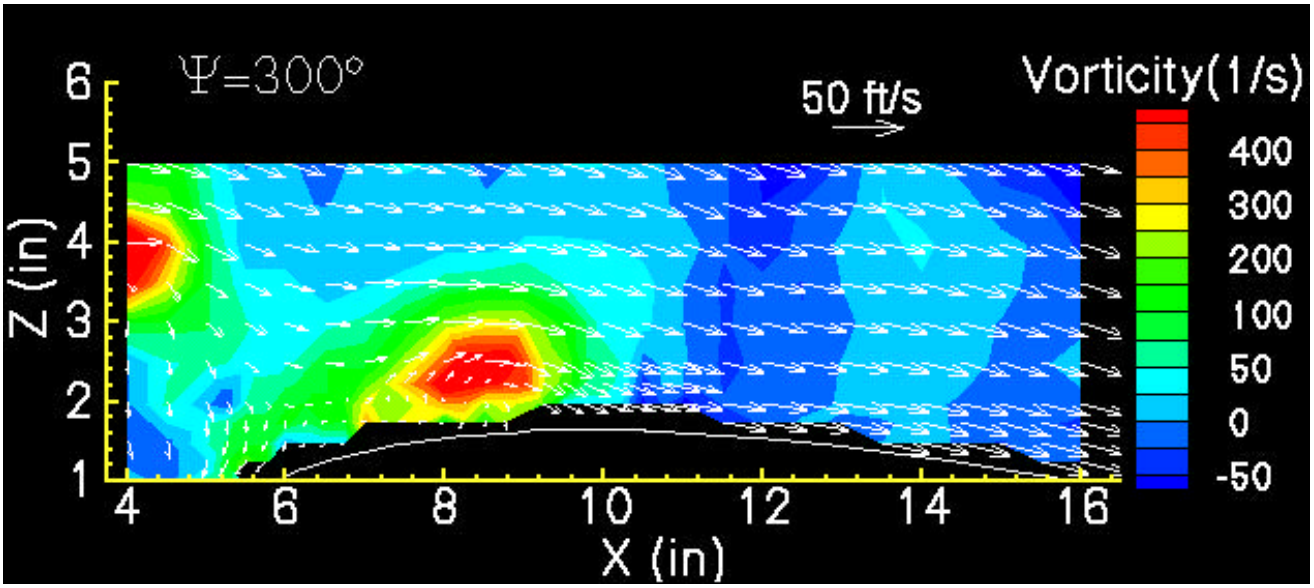

Figure 5a: 2 Dimensional velocities and vorticity in the y/R=0.0 plane

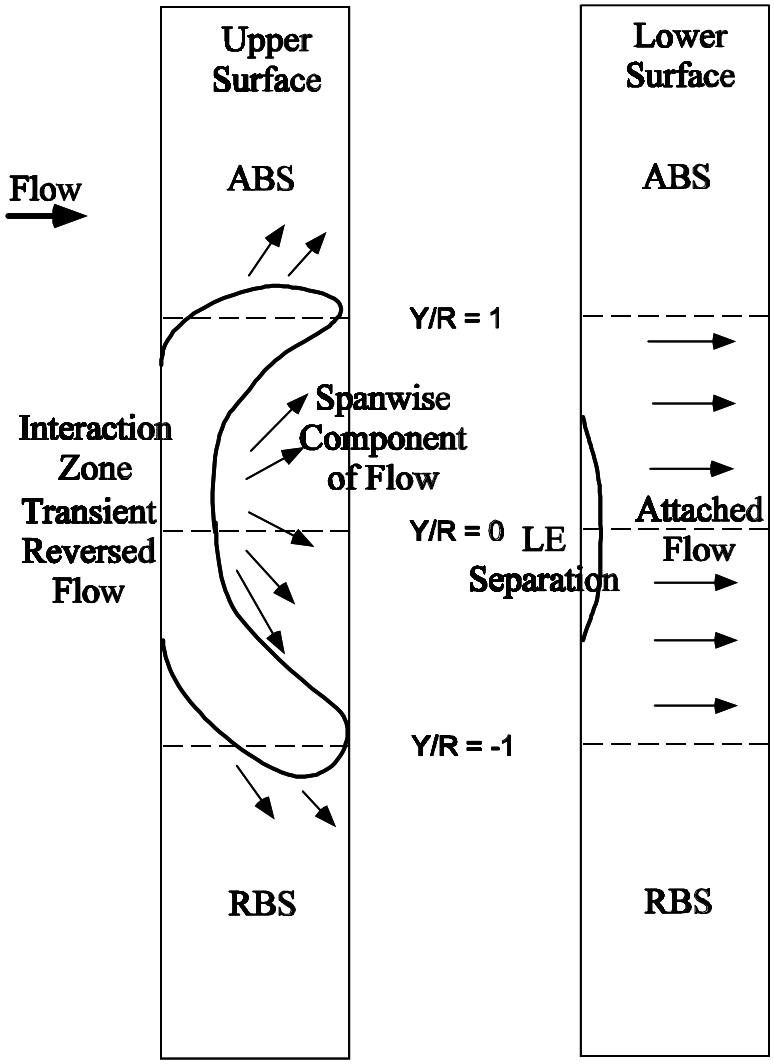

Figure 5b: Schematic of tuft visualization results

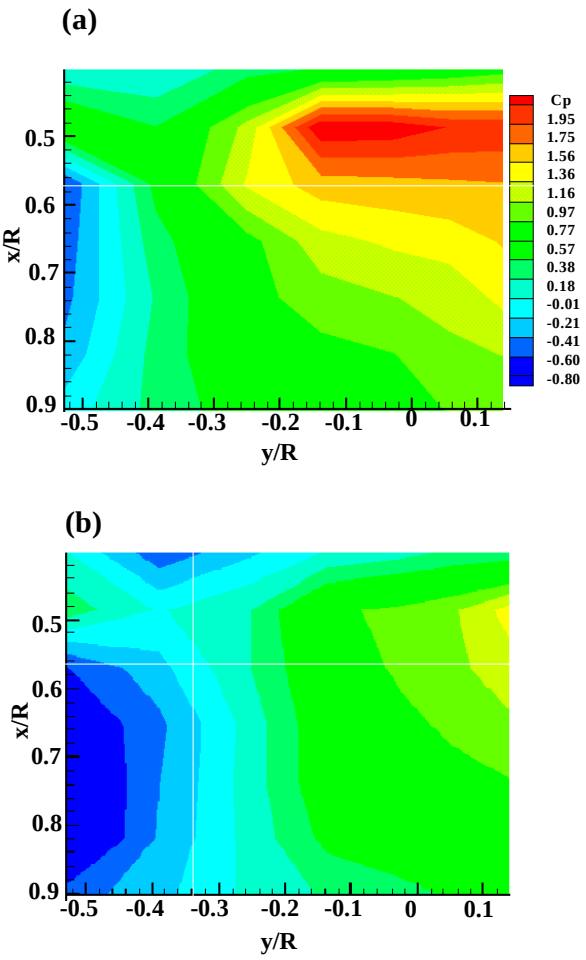

Figure 6: Static pressure contours over the wing upper surface with full span flap at a) 0° b) 27°

the measurement area, as expected. This surface pressure reduction can be clearly seen in Figure 7, which compares Cp along the chord at y/R=0.03 (close to mid-span). The pressure reduction due to flap deflection corresponds to a ΔCp of 1.4. The contours indicate a shift in the high pressure regions towards the ABS.

SCV measurements in the mid-span location suggested a skewing of the rotor wake towards the ABS, reinforcing the observation from Fig. 7.

It was shown earlier that there is a strong spanwise flow directed towards RBS downstream of the 3D separation line formed on the wing due to vortex interaction. By deflecting the flap and allowing the flow to deflect downstream this spanwise flow is reduced, thus shifting the rotor wake laterally.

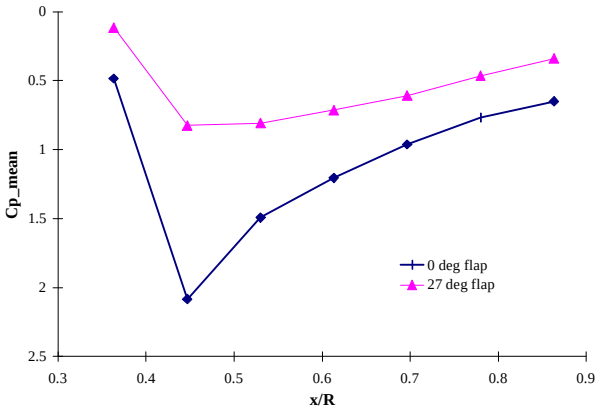

Figure 7: Chordwise distribution of Mean Cp at y/R=0.03.

Measurements were made at other locations to confirm this observation and are presented in the last section.

This shift in the rotor wake impingement on the wing was also seen with the segmented flap system. Fig. 8 shows the upper-surface Cp contours for several different flap combinations. The undeflected case is shown in Figure 8(a). A wake shift similar to the full span flap deflection case is seen in Figure 8(b) when all four segments are deflected 30 degrees. The vertical rotor-wing separation distance is increased to 0.92R. The pressures display an expected reduction in maximum Cp. Two other flap deflection configurations were performed as well. Deflecting only the two inboard flaps produced a shift in the pressure contours similar to that from the full span deflection. Deflecting only the two outboard flaps, however, showed little effect on the pressure contours.

2. Linear Reduction in download with flap deflection: Four compression/tension load cells were used to measure the loads on the wing. Loads were time averaged over 30 seconds for each setting. Figure 9 demonstrates download reduction on the wing with increasing deflection of all four flap segments. Data for 30 deg. inboard and outboard flap deflection are also shown. Flap effectiveness in download reduction is seen to linearly increase up to 30 deg. of deflection. Beyond 30 degrees, increasing flap angle does not significantly change the download on the wing, but does produce a large drag increase. Deflecting the outboard flaps alone was mildly effective, while inboard flaps were shown to be nearly as effective as full span

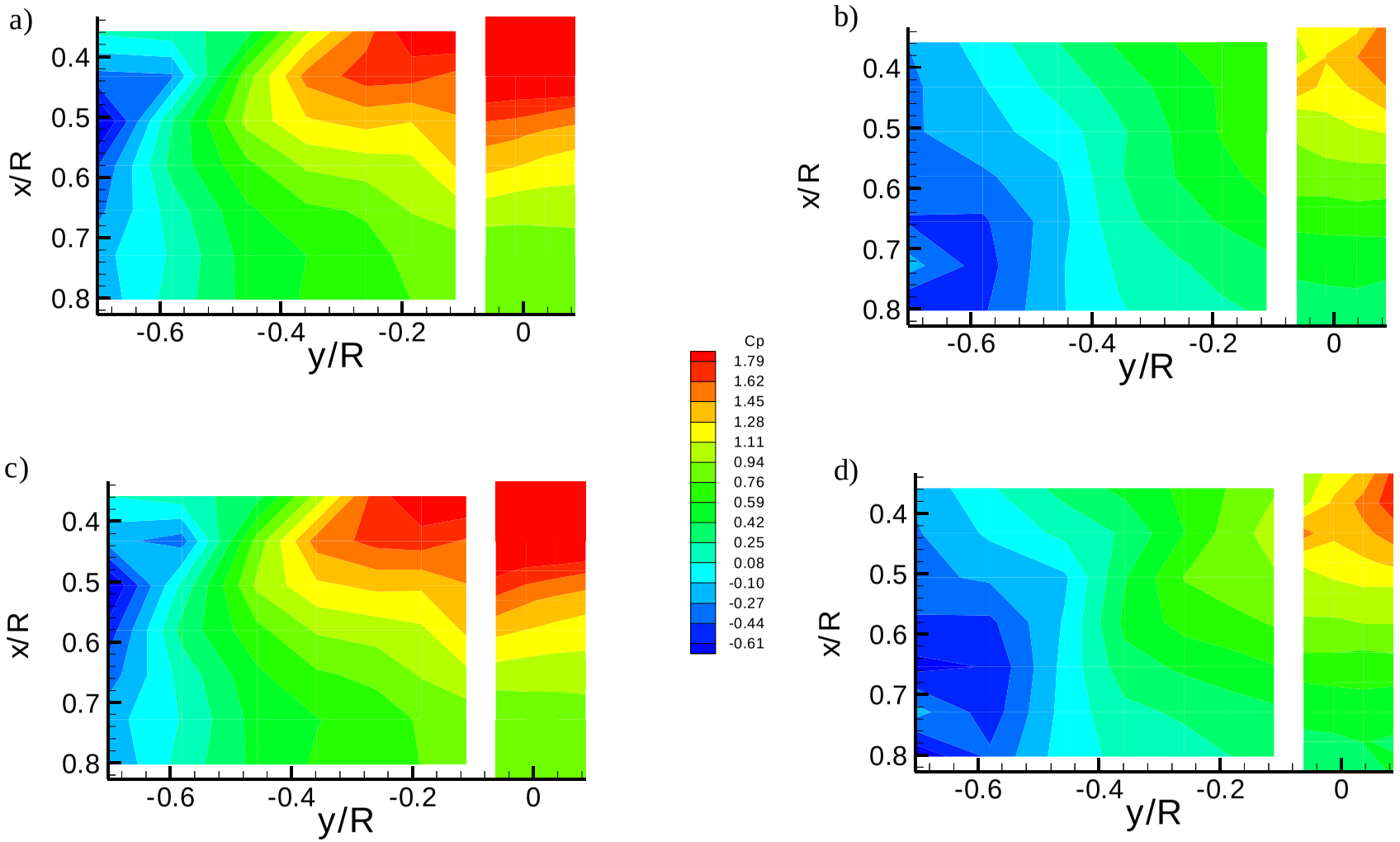

Figur e 8: Stat ic Press ure conto urs over the wing upper su rface wit h segment ed flap system at a) 0 deg. b) 30 de g. c) Outboa rd only flaps at 30 d eg. d) Inboar d only flaps a t 30 de g.

deflection. At an advance ratio of 0.075, full span flap deflection beyond 15 deg. changed the net wing force to lift.

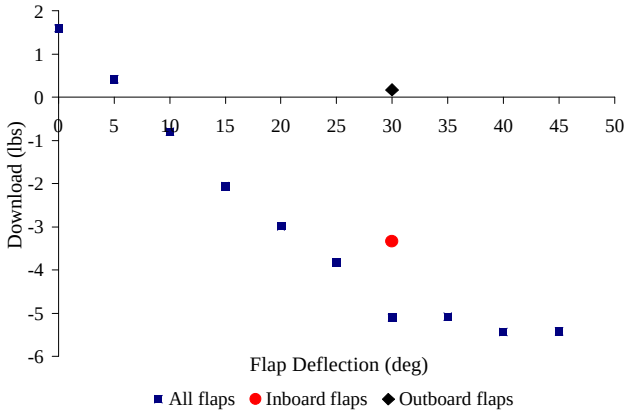

Figure 9: Variation on download on wing with flap deflection

3. ***Moment data analysis:*** Rolling moment about the wing's mid-span can be reconstructed from the load cell data since the distances from the center of the wing to the load cells are known. Table 1 shows the rolling moment generated by various flap deflections. Deflection of the flaps on the ABS side of the wing shows an appropriate RBS-down rolling moment.

Likewise, deflection of the RBS flaps generates an ABS-down rolling moment. Full span, inboard and outboard flap deflection all generated approximately the same net rolling moments, possibly due to the opposing moments from the ABS and RBS loads. However, the individual rolling moment contribution from the ABS and RBS load cells were much lower in magnitude for the outboard flap deflection case as expected. All flap configurations are at an advance ratio of 0.075.

Table 1: Rolling Moments Generated by Flap Deflection

Configuration	Rolling Moment (ft-lbs)
Zero flap deflection	2.19
Full span flap 30°	1.05
Inboard flaps 30°	1.53
Outboard flaps 30°	1.30
RBS flaps 30	3.93
ABS flaps 30°	-1.07

4.Unsteady velocity field data: Planar velocity measurements were made both on the ABS and RBS. The measurement area was about 0.8 m X 0.4 m, extending from the rotor hub to the wing centerline and beyond the full-span trailing edge flap. Data was recorded with the full span flap at 0 deg. and 27 deg. flap deflection angles. Several reliability criteria were applied to eliminate faulty vectors from the figures. This is the reason for the regions with no vectors in the 2D vector fields shown in Figures 10,11 & 12.

The velocity fields at two rotor azimuths (0 & 90 deg.) at the mid-span location are shown in Fig. 10a and 10b. With the flap deflected, the freestream component of velocity is increased for both rotor azimuths. Therefore the wake is pulled further downstream when compared to the zero deflection case. This cannot be seen clearly in the pressure contours, however, due to the limited wing surface area covered by the pressure taps. At the y/R=0.5 location on the ABS (Figure 11a) the flow is predominantly downflow and the decrease in the downflow velocities with flap deflection is clearly seen. The higher downwash velocities as compared to the mid-span location indicate wake skewing towards the ABS even when the flap is undeflected. This was previously reported [7] based on LDV measurements on a similar rotor-wing configuration. When the flap is deflected, the decrease in downwash velocities suggests wake skewing. By deflecting the flap and allowing the flow to deflect downstream, the spanwise flow is reduced, thus shifting the rotor wake laterally.

At the y/R=0.5 location on the RBS (Figure 11b), the flowfield resembles freestream flow with some downward deflection near the trailing edge. There is some evidence of flow reversal due to vortex interaction near the wing leading edge. However, the effect of flap deflection is not as marked as on the ABS. Near the edge of the rotor wake region at the y/R=1.0 location (Fig. 12) on the ABS there is a clear region of rotating flow near the wing leading edge. When the flap is deflected this region has moved further upstream thus increasing the separation between the two vortex trajectories. At the y/R=1.0 location on the RBS, the freestream component as well as the downwash velocity decrease with flap deflection.

CONCLUSIONS

The experiments reveal several features of the rotor wake/wing interaction that should pose interesting checks on prediction codes:

1. There is a strong n-per-rev loading on the wing due to the pressure distributions of the moving blades, and their interaction with the wing surface.
2. Wing interaction causes a large divergence in the trajectories of tip vortices from the different blades, so that the flowfield in fact shows a strong once-per-rev component superposed on the n-per-rev.
3. When the tip vortices reach the wing surface, they induce transient flow separation on the upper surface, as well as high levels of spanwise velocity downstream of the separation line. This appears to be the origin of the wall jet which build up the "fountain effect".
4. Deflection of a full-span flap causes a lateral shift of the wake and its impingement region on the wing.
5. Download appears to be reduced linearly with flap deflection up to 30 degrees, but offers little benefit for larger deflections in this test case.
6. The present experiments demonstrate the use of whole-field velocimetry, effectively combined with the force and pressure sensing required to quantify the problem over a wide range of test conditions required in rotorcraft testing.

ACKNOWLEDGMENTS

This work was performed under Tasks B09 and B10 of the of the NASA/Army Rotorcraft Center of Excellence at Georgia Tech. The technical monitors are Dr. Yung Yu and Dr. T.L. Doligalski.

REFERENCES

1 Felker, F.F., Light, J.S., "Aerodynamics Interactions Between a Rotor and Wing in Hover", Journal of the American Helicopter Society, Vol. 33, No. 2, April 1988.

2. Funk, R.B., Komerath, N.K., "Rotor Wake Interaction with a Lifting Surface". Proceedings of the American Helicopter Society Annual Forum, Ft. Worth, TX, May 1995.

3. Funk, R.B., “Transient Interactions Between a Rotor Wake and a Lifting Surface”, Ph.D. Thesis, School of Aerospace Engineering, Georgia Institute of Technology, 1995.

4. Fawcett, P.A., Komerath, N.M., “Spatial Correlation Velocimetry in Unsteady Flows”, AIAA 91-0271, Jan. 1991.

5. Fawcett, P.A., Funk, R.B., Komerath, N.M., “Quantification of Canard and Wing Interactions Using Spatial Correlation Velocimetry”, AIAA92-2687, June 1992.

6. Funk, R.B., Fawcett, P.A., Komerath, N.M., “SCV Measurements in the Wake of a Rotor in Hover and Forward Flight”, AIAA paper 93-03080, July 1993.

7. Griffin, M.H., Funk, R.B., Komerath, N.M., “Wind Turbulence Measurement over Large Areas Using Spatial Correlation Velocimetry”, Proceedings of the Silver Symposium of the Flight Test Engineers Society V-4-12, Aug. 94.

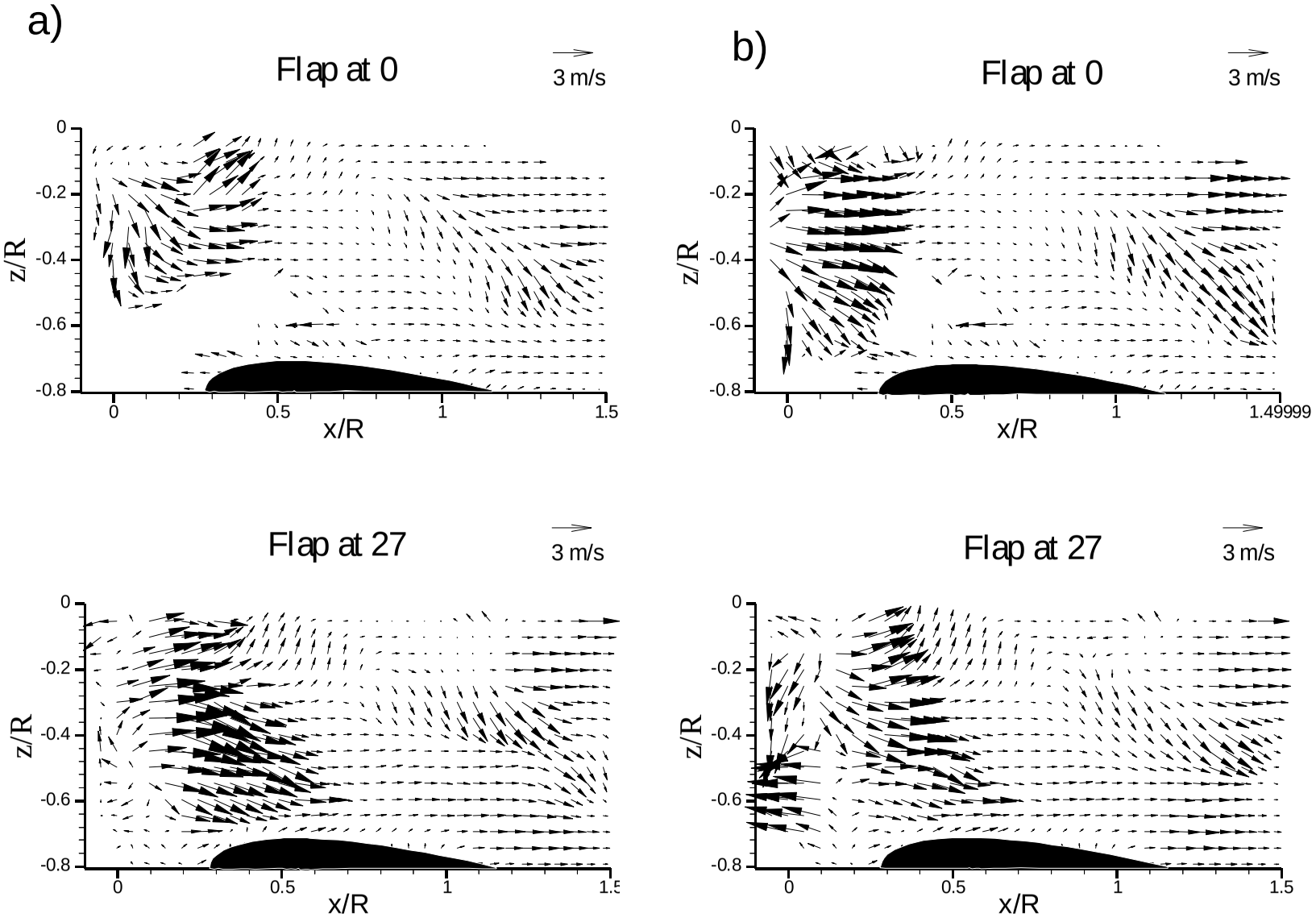

Figure 10: Two-dimensional velocity fields at y/R=0 midspan location, at a) 0 and b) 90 deg. rotor azimuth

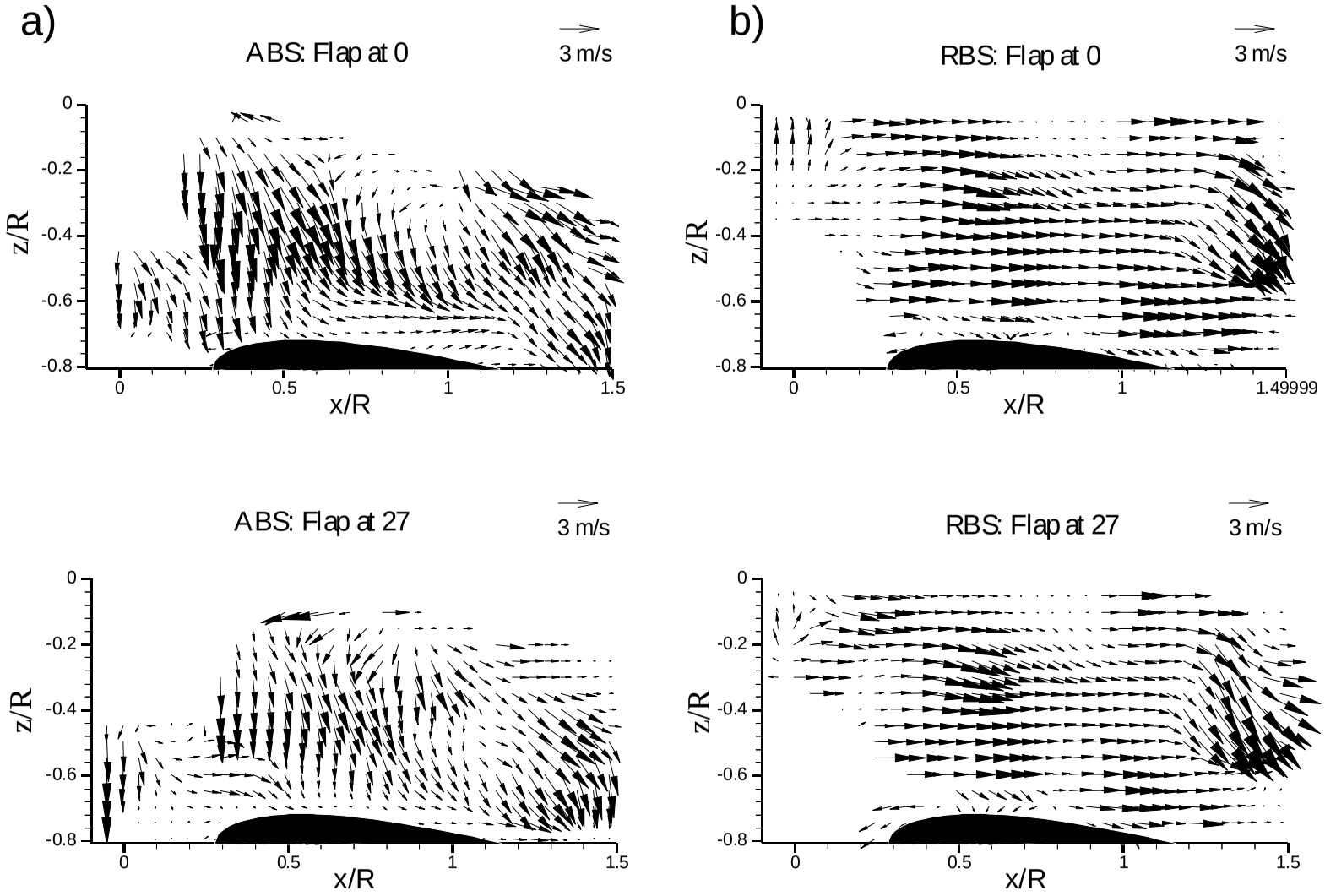

Figure 11: Two-dimensional velocity fields at
y/R=0.5 location on (a) ABS and b) RBS at 90 deg. rotor azimuth

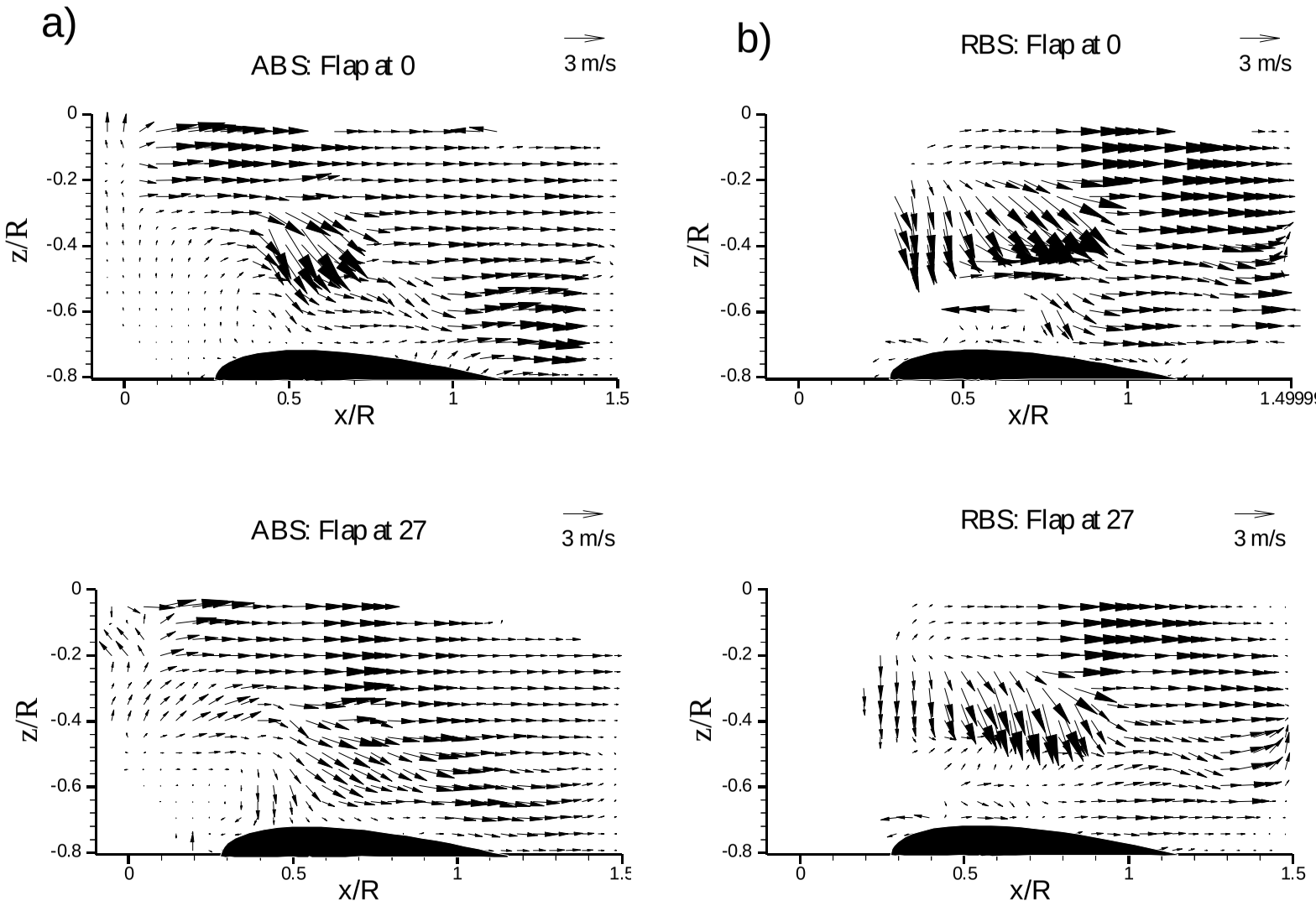

Figure 12: Two-dimensional velocity fields at y/R=1.0 location on a)ABS and b)RBS at 90 deg. rotor azimuth